RESEARCH PAPER

In Vitro and *In Silico* Strategies to Identify OATP1B1 Inhibitors and Predict Clinical Drug–Drug Interactions

Maria Karlgren · Gustav Ahlin · Christel A. S. Bergström · Richard Svensson · Johan Palm · Per Artursson

ABSTRACT

Purpose To establish *in vitro* and *in silico* models that predict clinical drug–drug interactions (DDIs) with the OATP1B1 (*SLCO1B1*) transporter.
Methods The inhibitory effect of 146 drugs and drug-like compounds on OATP1B1-mediated transport was studied in HEK293 cells. A computational model was developed to predict OATP1B1 inhibition. Concentration-dependent effects were investigated for six compounds; clinical DDIs were predicted by calculating change in exposure (i.e. *R*-values) in eight different ways.
Results Sixty-five compounds were identified as OATP1B1 inhibitors at 20 μM. The computational model predicted the test set with 80% accuracy for inhibitors and 91% for non-inhibitors. *In vitro–in vivo* comparisons underscored the importance of using drugs with known clinical effects as references. Thus, reference drugs, cyclosporin A, gemfibrozil, and fenofibrate, provided an inhibition interval to which three antiviral drugs, atazanavir, lopinavir, and amprenavir, could be compared and their clinical DDIs with OATP1B1 classified.
Conclusions Twenty-two new OATP1B1 inhibitors were identified, a predictive OATP1B1 inhibition *in silico* model was developed, and successful predictions of clinical DDIs were obtained with OATP1B1.

ABBREVIATIONS

ABC	ATP-binding cassette
AUC	area under the plasma-concentration time curve
BCRP	breast cancer resistance protein
DDI	drug–drug interaction
E17βG	estradiol-17β-glucuronide
E3S	estrone-3-sulphate
ESI	electrospray ionization
F_a	fraction absorbed
FBS	fetal bovine serum
F_u	fraction unbound
HBSS	Hank's balanced salt solution
HEK293	human embryonic kidney 293 cells
HMG-CoA	3-hydroxy-3-methylglutaryl-coenzyme A
$I_{in,max}$	maximal inhibitor concentration at the inlet of the liver
I_{max}	maximal systemic plasma concentration of the inhibitor
k_a	absorption constant
MDR1	multi-drug resistance protein 1
MQ	Milli-Q
MRP	multi-drug resistance associated protein
NTCP	Na$^+$-taurocholate co-transporting polypeptide
OATP	organic anion transporting polypeptide
OPLS-DA	orthogonal partial least squares projection to latent structures discriminant analysis
PCR	polymerase chain reaction
Pgp	P-glycoprotein
Q_h	hepatic blood flow
SLC	solute carrier
UPLC-MS/MS	ultra performance liquid chromatography-tandem mass spectrometry

M. Karlgren (✉) · G. Ahlin · C. A. S. Bergström · R. Svensson · P. Artursson
Uppsala University Drug Optimization and Pharmaceutical Profiling Platform, Department of Pharmacy, Uppsala University
The Biomedical Centre, P.O. Box 580, 751 23 Uppsala, Sweden
e-mail: maria.karlgren@farmaci.uu.se

J. Palm
AstraZeneca Research and Development
Mölndal, Sweden

INTRODUCTION

The liver-specific organic anion transporting polypeptide 1B1, OATP1B1 (*SLCO1B1*), is one of the highest expressed uptake transporters in the human hepatocyte (1,2). It is localized in the basolateral membrane of the hepatocyte and translocates substrates from the bloodstream into the hepatocyte. The significance of OATP1B1 has recently been emphasized by its inclusion as one of seven transporters of considerable importance for drug disposition (3). In that paper, authored by the International Transporter Consortium, criteria for the identification of important elimination routes are given, along with predictive decision trees and suggestions for the extrapolation of the *in vitro* OATP1B1 results to the *in vivo* situation. OATP1B1 has previously been shown to interact predominantly with negatively charged compounds (4,5) and is known to transport a number of drugs, e.g. 3-hydroxy-3-methylglutaryl-coenzyme A (HMG-CoA) inhibitors (statins), bosentan and repaglinide (6–8). In addition, it mediates the transport of several endogenous compounds, such as bile acids, in parallel with, e.g., the bile acid transporter Na$^+$-taurocholate co-transporting polypeptide (NTCP, *SLC10A1*) (9,10). In concert with the efflux transporter multi-drug resistance associated protein 2 (MRP2, *ABCC2*), which is positioned in the apical membrane of the hepatocyte, it has been suggested that OATP1B1 is involved in active vectorial transport of compounds from the blood to the bile (11).

Several drugs inhibit OATP1B1-mediated transport, which may result in lower hepatic intracellular and higher blood concentrations of OATP1B1 substrates (2,12,13). The importance of OATP1B1 in drug transport is underlined by its involvement in drug–drug interactions (DDIs) described throughout the literature (6,7,14). For instance, the area under the curve (AUC) of the OATP1B1 substrate rosuvastatin was increased 7.1 times when co-administered with the OATP1B1 inhibitor cyclosporin A (14). *In vitro* models suggested that the observed increase in the AUC was related to the inhibition of OATP1B1 (14). Similarly, DDIs with OATP1B1 have been shown for rifampicin and botensan (8,15), and OATP1B1 may also be involved in the reported DDIs of gemfibrozil and a number of statins (7).

The observations of DDIs at the OATP1B1 level have called for reliable and easy-to-use models to make it possible to identify such DDIs already in the pre-clinical stage. Indeed, a number of experimental *in vitro* models have been used with some success to investigate inhibition of the OATP1B1 transporter (13,14,16). In addition, tools combining *in vitro* and *in silico* models for the potential identification of DDIs in the early phases of the drug discovery process have been described (17). However, as yet, no extensive systematic study has been conducted on drug–drug interactions with OATP1B1.

Previously, we developed experimental and computational models for efflux (multi-drug resistance protein 1 (MDR1 or

Pgp, *ABCB1*), breast cancer resistance protein (BCRP, *ABCG2*) and MRP2) and uptake (organic cation transporter 1 (OCT1, *SLC22A1*)) transporters (18–21), all of which are of considerable importance for hepatic drug transport and clearance. For these transporters, optimized *in vitro* methods were developed, and experimental data for large datasets of compounds were generated to aid in the development of predictive *in silico* models. Here, we describe an *in vitro* screening assay for the rapid assessment of OATP1B1 inhibition and then present an application of this assay to the investigation of the inhibition potential of 146 drugs and drug-like compounds. We then use the experimental data to develop a computational model for the prediction of OATP1B1 interactions. Finally, we make *in vitro–in vivo* extrapolations by calculating the so-called *R*-values (i.e. the predicted change in exposure of a drug) using recently published procedures (3,22) and predicted clinical DDIs involving OATP1B1 for a dataset of six compounds using the specific substrate atorvastatin. Our results emphasize the DDI potential of OATP1B1 and add to the existing evidence supporting the usefulness of rather simple *in vitro* and *in silico* tools for the identification of DDIs with transport proteins.

MATERIALS AND METHODS

Compounds

A dataset of 146 compounds was used for the investigation. A list of suitable candidates was compiled from a model dataset for transporter interaction studies (21), and this list was extended with compounds known to interact with OATP1B1 and/or MRP2 (21), bile acids and three therapeutic groups of interest for OATP1B1: statins, protease inhibitors and anti-diabetic compounds. The substances were obtained from Sigma-Aldrich (St. Louis, MO), International Laboratory USA (San Bruno, CA), 3B Scientific Corporation (Libertyville, IL) and AstraZeneca R&D Mölndal (Sweden). Radiolabeled estradiol-17β-glucuronide (E17βG) was obtained from PerkinElmer (Waltham, MA).

Construction of an OATP1B1 Expression Vector

The *SLCO1B1*/OATP1B1 open reading frame was obtained using restriction digestion with *Kpn*I/*Xho*I from an *SLCO1B1*/OATP1B1-pcDNA3.1 expression vector (kindly provided by Dr Lena Gustavsson, AstraZeneca R&D Lund, Sweden). The resulting DNA fragment was cloned into the corresponding restriction sites of the expression vector pcDNA5/FRT (Invitrogen, Carlsbad, CA). The inserted sequence was verified by DNA sequencing analysis (Uppsala Genome Center, Uppsala, Sweden).

Establishment of Stable Clones and Cell Cultivation

Human embryonic kidney cells Flp-In-293 (Invitrogen, Carlsbad, CA) were transfected with the pOG44 vector (Invitrogen, Carlsbad, CA) and with the constructed OATP1B1-pcDNA5/FRT expression vector or empty pcDNA5/FRT vector (mock) using Lipofectamine 2000 (Invitrogen, Carlsbad, CA) according to the manufacturer's recommendations. Stable clones were obtained by selection using Flp-In-293 medium (Dulbeccos's modified eagle's medium supplemented with 10% fetal bovine serum (FBS) and 2 mM L-glutamate) supplemented with 75 µg/ml of Hygromycin B (Invitrogen, Carlsbad, CA). For continued culturing, the stable clones were cultivated in Hygromycin B supplemented Flp-In-293 medium.

All cells were cultured at 37°C in an atmosphere of 95% air and 5% CO_2 and sub-cultured twice a week. Passage numbers 5 to 30 were used throughout the study. All cell culture media and reagents were obtained from Invitrogen (Carlsbad, CA) or Sigma-Aldrich (St.Louis, MO).

Two to 3 days prior to performing the transport experiments, cells were seeded in black 96-well poly-D-lysine coated plates (Greiner, Frickenhausen, Germany) or CellBind plates (Corning, Amsterdam, Netherlands) (experiments using E17βG as substrate), or 24-well Cell-Bind plates (Corning, Amsterdam, Netherlands) (experiments conducted using atorvastatin as the substrate) at a density of 30,000–60,000 (96-well plates) or 600,000 cells/well (24-well plates). The cell density was optimized using computer-assisted experimental design conducted with MODDE 7.0 (Umetrics, Umeå, Sweden) as described below.

Transport and Inhibition Studies

In the transport studies, described below, all experiments were performed in at least triplicate. Common to all experimental protocols was the following procedure: before starting the experiment, cells were washed twice with pre-warmed HBSS with pH 7.4, followed by incubation at 37°C with pre-warmed test solutions. The transport experiments were terminated by adding ice-cold buffer, followed by four washing steps. Total protein content was measured using the BCA Protein Assay Reagent Kit (Pierce Biotechnology, Rockford, IL) according to the manufacturer's instructions. In all experiments, mock-transfected cells were included on each plate to correct for the passive permeability.

Characterization of the OATP1B1 Transport

The cells grown in the 96-well plates were incubated with a solution containing 1 µCi/ml (24 nM) ^{3}H-estradiol-17β-glucuronide (^{3}H-E17βG) and 1–200 µM of

unlabeled E17βG in HBSS, and then analyzed using a liquid scintillation counter as described below to determine K_m and V_{max} of the model substrate E17βG, which was used as a substrate in single point inhibition experiments. The K_m and V_{max} of atorvastatin, the specific substrate used in the *in vitro–in vivo* extrapolation experiments, were determined using cells grown in 24-well plates. The cells were incubated with a solution containing 0.2–50 µM atorvastatin in HBSS and analyzed using UPLC-MS/MS as described below. Uptake kinetics were assessed by plotting the initial uptake rate (uptake after 1 min) against the substrate concentration [S]; apparent K_m and V_{max} were determined by non-linear regression (using Prism v.4.02 from GraphPad, San Diego, CA) fitted to Eq. 1:

$$v = \frac{V_{max}[S]}{K_M + [S]} + Pdif \times [S] \qquad (1)$$

where P*dif* is the passive permeability of the substrate. Substrate concentrations well below or close to the K_m were selected for future studies using E17βG or atorvastatin, respectively.

Screening for Inhibition of OATP1B1-Mediated Transport

Screening for inhibition of OATP1B1-mediated transport was achieved by performing single point inhibition measurements. Experimental design, as implemented in MODDE 7.0 (Umetrics, Umeå, Sweden), was used for optimizing the assay with regard to the substrate concentration, amount of labeled substrate, incubation method, cell seeding density, and number of days in culture before the experiments (18). Within the experimental design, the results from the OATP1B1 transport characterization were considered for the optimization of the substrate concentration and incubation time. In summary, in the screening assay, cells that were grown in 96-well plates were incubated for 5 min with a solution containing 20 µM of the test compound, 1 µCi/ml (24 nM) ^{3}H-E17βG and 0.5 µM E17βG in HBSS. The strong inhibitor estrone-3-sulphate (E3S) was included on each plate as a control. OATP1B1 cells incubated without a potential inhibitor were used as the reference for the calculations of the inhibitory percentage of the compounds under investigation. A compound was classified as an OATP1B1 inhibitor if it inhibited the uptake of E17βG by more than 50% (18,21).

Establishment of IC50 Curves

Cells grown in 24-well plates were incubated for 2 min with a test solution containing 1 µM atorvastatin to enable

inhibition curves to be derived for the six selected *in vivo* OATP1B1 inhibitors and non-inhibitors: cyclosporin A (0.01–25 µM), gemfibrozil (0.01–500 µM), fenofibrate (0.1–100 µM), atazanavir (0.01–100 µM), amprenavir (0.01–500 µM) or lopinavir (0.01–10 µM). The intracellular atorvastatin content was analyzed using UPLC-MS/MS as described below. The passive uptake in mock cells was subtracted from the total uptake in the OATP1B1 expressing cells at each inhibitor concentration. IC_{50} was determined and the apparent K_i (assuming the kinetics appropriate for competitive inhibition) calculated using Prism version 4.02 (GraphPad, San Diego, CA).

Liquid Scintillation Analysis

Immediately after the final washing steps in the transport experiments, the cells incubated with radioactive E17βG were trypsinized, lysed using 1 M NaOH, and then neutralized using 1 M HCl. Thereafter, the intracellular concentrations were analyzed with an Ultima Gold scintillation cocktail (PerkinElmer, Shelton, CT) using a Beckman LS6000IC liquid scintillation counter (Beckman Coulter, Fullerton, CA).

UPLC-MS/MS Analysis

After the final washing steps, the cells incubated with atorvastatin were dried, and extracted using 0.2 mL AcN: H_2O 60:40 spiked with 50 nM warfarin as the internal standard, which was followed by centrifugation at 3,500 rpm for 20 min using a 5810R centrifuge from Eppendorf (Hamburg, Germany). Thereafter, the supernatants were subjected to UPLC-MS/MS analysis of intracellular atorvastin concentrations using the following analytical system: UPLC (Waters, Milford, MA) coupled to a Thermo Quantum Discovery triple quadrupole with ESI interface, with a reversed phase C18 column (particle size of 1.7 µm) (Waters, Milford, MA) and a mobile gradient consisting of acetonitrile, formic acid and MQ-water.

Calculation of *R*-Values and *In Vitro* to *In Vivo* Drug–Drug Interaction Predictions

For the five selected compounds (including three inhibitors and two non-inhibitors *in vivo*) where an IC_{50} and K_i value could be obtained, an *in vitro–in vivo* extrapolation was conducted by calculating the changes in drug exposure, i.e. the *R*-values, with or without these five selected compounds, through the use of both Eqs. 2 and 3:

$$R = 1 + \frac{F_u * I_{in,max}}{IC_{50}} \tag{2}$$

$$R = 1 + \frac{F_u * I_{in,max}}{K_i} \tag{3}$$

in which F_u is the fraction unbound, obtained from the maximal inhibitor concentration at the inlet of the liver, $I_{in,max}$, which was calculated using Eq. 4 (3,22):

$$I_{in,max} = I_{max} + \frac{F_a * Dose * k_a}{Q_h} \tag{4}$$

where F_a is the fraction absorbed (equal here to the maximum reported oral bioavailability (23–25), or set to 1 for the purpose of comparison with previous *in vitro–in vivo* extrapolations (3)). For lopinavir, no data could be identified for the bioavailability, so only a value of $F_a = 1$ could be used. The dose is the maximum oral dose given, I_{max} is the maximal systemic plasma concentration (obtained from (24–28)), k_a is the absorption constant (here, set to 0.03 or 0.1 (22,29)), and Q_h is the hepatic blood flow (1.5 l/min (3)). Equation 3, using K_i for *R*-extrapolation, was used by Hirano and co-workers in a paper from 2006 (22), in which the authors recommended setting the F_a equal to 1 and using a value of $k_a = 0.1$ to estimate the maximum $I_{in,max}$. In contrast, the recent paper from the International Transporter Consortium uses Eq. 2, IC_{50} and $k_a = 0.03$ for the *R*-extrapolation (3). In the latter publication, no recommendation is made regarding F_a, although $F_a = 1$ is used for the examples provided by the authors. Using these approaches and equations, as well as combining different values for the fraction absorbed (F_a) and the absorption rate constant (k_a), as indicated above, a total of eight *R*-values were obtained for each compound. A mean *R*-value was calculated for each compound for use in comparisons with clinical data.

Molecular Descriptors

Three-dimensional molecular structures were generated from SMILES representations using Corina, version 3.0 (Molecular Networks, Erlangen, Germany), and were used as the input for molecular descriptor calculations performed with DragonX, version 1.4 (Talete, Milan, Italy), ADMETPredictor, version 5.0 (SimulationsPlus, Lancaster, CA), and SELMA (AstraZeneca R&D, Mölndal, Sweden). A total of 91 molecular descriptors representing the molecular size, flexibility, connectivity, polarity, and hydrogen bonding potential, all of which had previously been used for predictions of transport protein interactions (20,21), were used in the computational modeling procedure.

Computational Modeling

Every third compound when the compounds were listed alphabetically was included in the test set and kept out of the model development. The remaining compounds were

included in the training set used for *in silico* modeling. A multivariate discriminant analysis was performed to separate inhibitors from non-inhibitors and to identify the critical molecular properties causing transporter inhibition. The two resulting datasets consisted of 98 compounds (including 44 inhibitors) in the training set and 48 compounds (of which 21 were inhibitors) in the test set. This resulted in a test set that was well covered by the training set used with regard to inhibitory effect and chemical structure, as shown by a principal component analysis using SIMCA-P+ version 11.0 (Umetrics, Sweden). However, in the five first principal components of the PCA of the chemical space, which together described 78% of the chemical variation of the dataset, bromosulfalein, cholecystokinin octapeptide and levothyroxine were identified as outliers. These compounds were, therefore, excluded from the training set to avoid biasing the model. Orthogonal partial least squares projection to latent structures, discriminant analysis (OPLS-DA), as implemented by SIMCA-P+ version 11.0, was used to obtain computational models for the separation of OATP1B1 inhibitors from non-inhibitors. Inhibitors were given the value 1 and non-inhibitors the value −1. The descriptors generated by DragonX were used as the input for the computational modeling. Charge was not included as a descriptor, since the charge descriptor, generated by different software, will be largely dependent on the accuracy of the pKa prediction, a property for which the predictions vary greatly from software to software. Instead, we took the simple approach of using only generally available DragonX descriptors (that do not cover charge descriptors) as the input for the model. A variable selection procedure was used in which groups of molecular descriptors that did not contain information relevant to the problem (i.e. noise) or which overlapped with other descriptors in their information content (as identified through proximity in the OPLS loading plots of the resulting models) were removed in a stepwise manner to optimize the model performance and to ensure that the final model would be transparent. If the molecular descriptors remaining in the model resulted in a prediction >0, the compound was classified as an inhibitor, whereas a negative value predicted the compound to be a non-inhibitor of OATP1B1. We excluded descriptors from the model if their removal resulted in improved or unaltered discrimination between inhibitors and non-inhibitors in the training set.

RESULTS

Characteristics of the Dataset

The dataset investigated is within the chemical space for prescribed oral drugs. Inclusion of compounds already known to interact with OATP1B1 and compounds with related structures to known inhibitors skewed the charge distribution of the dataset towards anionic drugs. This was deliberate, as it was intended to enrich the dataset with compounds likely to interact with OATP1B1. The range of the molecular weight of the compounds was from 108.1 (quinone) to 1202.8 (cyclosporin A), with a mean value of 428.0 (±140.4) g/mol (Fig. 1a). This is higher than the mean value of 343.7 g/mol for marketed low-molecular-weight drugs (30). Further, as shown in Fig. 1b, the lipophilicity (logP) of the dataset ranged between −7.0 (acarbose) and 7.4 (tipranavir), with a mean value of 2.90 (±1.65). The topological polar surface area ranged between 3.2 (amitriptyline) and 434.0Å^2 (cholecystokinin octapeptide (CCK-8)) with a mean of 106.9Å^2 (±52.5), as displayed in Fig. 1c. The mean lipophilicity and polar surface area in the dataset were similar to the mean values reported for registered oral drugs. Thirty-two percentages of the compounds were neutral, 39% were anions and 25% were cations (Fig. 1d) at pH 7.4.

Establishment of OATP1B1 Cell Models

The deduced amino acid sequence for the *SLCO1B1/OATP1B1*-pcDNA5/FRT construct was found to be identical with the OATP1B1 wild-type variant, i.e. the *SLCO1B1*1a* allele. Real-time PCR and Western blot analyses showed that the OATP1B1 mRNA and protein were specifically expressed in the OATP1B1 transfected cells and that the OATP1B1 protein was localized at the plasma membrane (data not shown).

Estradiol-17β-Glucuronide and Atorvastatin Transport Kinetics

The uptake of E17βG was linear over the first 10 min, and the uptake of atorvastatin was linear for 2 min (data not shown). All uptake experiments were performed in the linear interval, with the chosen durations being 5 min and 2 min for E17βG and atorvastatin, respectively. At the end of these periods, the uptake of E17βG and atorvastatin in the OATP1B1 cells was at least 8 and 3 times higher than the values obtained in mock-transfected cells, respectively. OATP1B1-expressing cells exhibited a K_m for E17βG of 12.85 (± 2.40) μM and a V_{max} of 1.37 (± 0.12) pmol/min/mg protein (Fig. 2a). For atorvastatin, a K_m of 0.77 (± 0.24) μM and a V_{max} of 6.61 (± 1.24) pmol/min/μg protein were obtained (Fig. 2b).

OATP1B1 Interaction and Characteristics of the Inhibitors

In the interaction studies, 65 of the 146 compounds analyzed (44.5%) inhibited the transport of E17βG by 50% or more at 20 μM and were therefore classified as
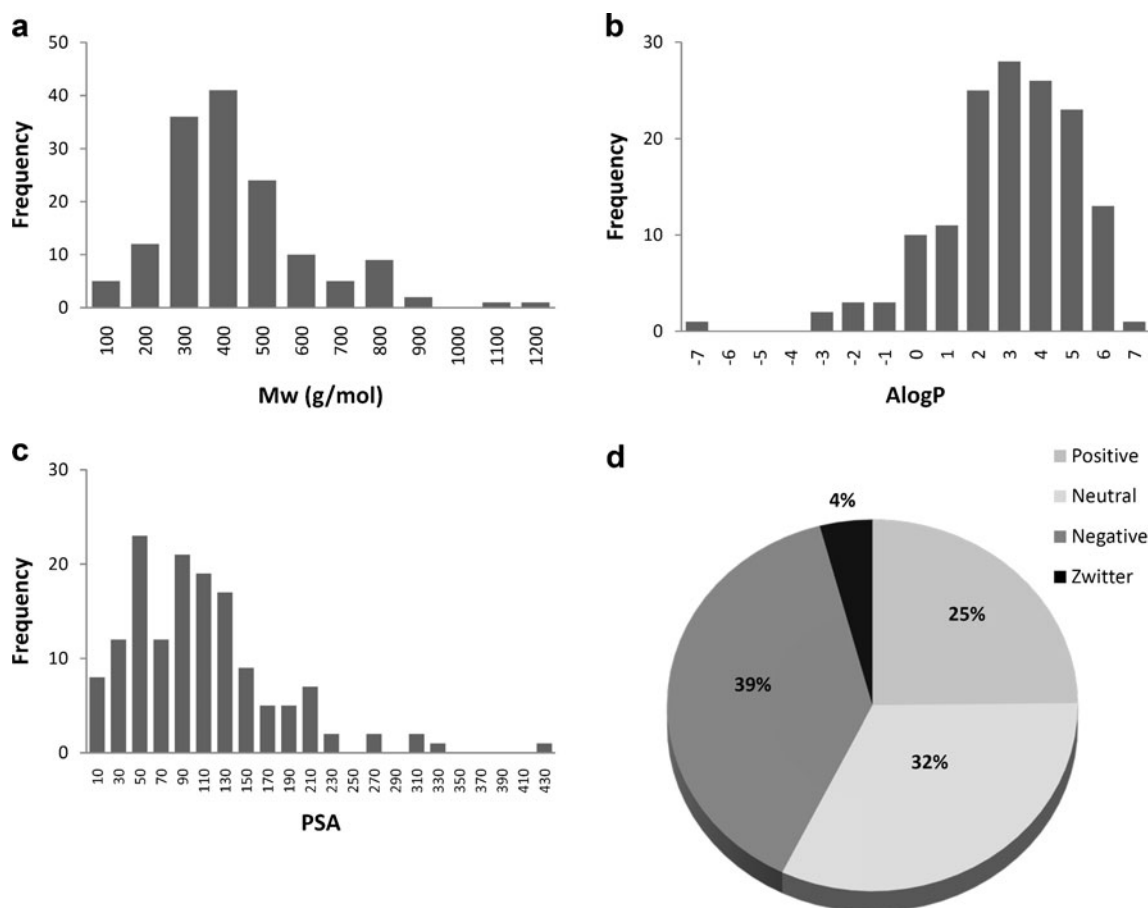
Fig. 1 The frequency distribution of the molecular properties of the dataset investigated for OATP1B1 inhibition. The distribution of molecular weight (**a**), AlogP (lipophilicity) (**b**), polar surface area (PSA) (**c**) and compound net charge at physiological pH (**d**) for the investigated compounds in the dataset.

OATP1B1 inhibitors (Fig. 3a, Table I). Of the inhibitors identified, as many as 22 were identified that had not been reported to interact with OATP1B1 previously. These included 5-CFDA, adefovir, candesartan, diclofenac, diethylstilbestrol, dipyridamole, GF120918, glycochenodeoxycholate, glycodeoxycholate, indomethacin, ivermectin, nicardipine, N-methylnicotinamide, nystatin, quinine, reserpine, spironolactone, sulfasalazine, taurochenodeoxycholate, taurodeoxycholate, tipranavir and vinblastine. The inhibitors identified were larger than the non-inhibitors, as shown by the difference in the mean molecular weight of the inhibitors (528.0±151.4 g/mol) and non-inhibitors (347.8±103.4 g/mol) (Fig. 3b). Fifty-eight percent of the inhibitors carried a negative charge at pH 7.4, in contrast to only four positively charged inhibitors (6%): GF120918, quinine, erythromycin and rosiglitazone (Fig. 3c). This enrichment of negatively charged compounds among the inhibitors and the presence of only low numbers of positively charged OATP1B1 inhibitors are significantly different from the charge distribution seen for all 146 compounds analyzed. Three known OATP1B1 substrates were not identified as inhibitors in our assay: penicillin G,

phalloidin, and levothyroxin (31–33). When investigated at higher concentrations (75 and 100 µM), an increased inhibition of E17βG uptake was observed for all three compounds (data not shown). At both 75 and 100 µM, levothyroxin would actually be classified as an inhibitor (i.e. >50% inhibition). Phalloidin, on the other hand, is a borderline compound, only reaching 49% inhibition (±13%) at a concentration of 100 µM, whereas even at 100 µM, penicillin G is classified as a non-inhibitor only inhibiting OATP1B1 to 32 (±18)%.

All statins (*n*=8) and protease inhibitors (*n*=7) inhibited OATP1B1 to more than 50% (Table I), whereas seven of the eight bile acids and three of the nine anti-diabetic compounds examined (rosiglitazone, repaglinide, glibenclamide) were classified as OATP1B1 inhibitors at 20 µM (Table I). The latter is in accordance with previous *in vitro* and *in vivo* studies identifying rosiglitazone, repaglinide, and glibenclamide as inhibitors and metformin and tolbutamide as non-inhibitors (22,34,35).

A substrate overlap has been suggested for OATP1B1 and the ABC transporter MRP2, (*ABCC2*) (11), but a corresponding overlap between OATP1B1 and MRP2
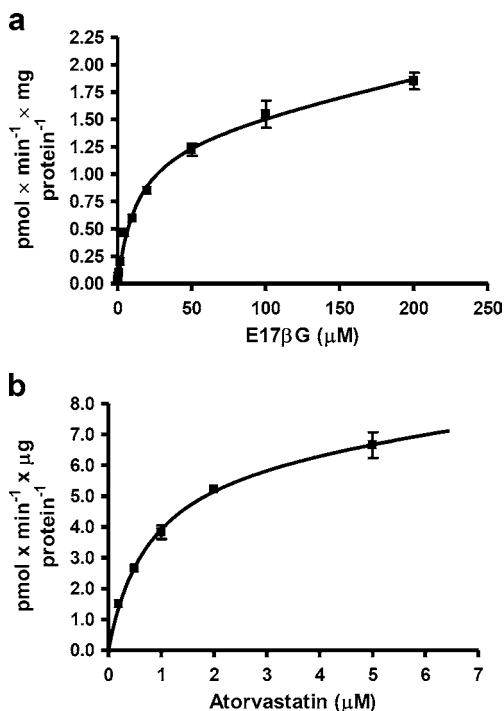
Fig. 2 Michaelis-Menten kinetics of uptake in HEK293 cells stably expressing the OATP1B1 transporter. Cells grown in 96-well plates were incubated with 1–200 μM estradiol-17β-glucuronide (E17βG) and 1 μCi/ml of ^{3}H-E17βG at 37°C. The intracellular accumulation of ^{3}H-E17βG was measured using a scintillation counter and the results presented here as the uptake in pmol per minute and per mg total protein (**a**). Each data point represents the mean uptake $\pm$ standard deviation ($n=3$). Cells grown in 24-well plates were incubated with 0.2–5 μM atorvastatin at 37°C. The intracellular accumulation of atorvastatin was measured using UPLC-MS/MS analysis and results presented here as the uptake in pmol per minute and per μg total protein (**b**). Each data point represents the mean uptake $\pm$ standard deviation ($n=2$).

inhibitors could not be observed for the 42 compounds in this study that were previously identified as inhibitors of the MRP2 transporter (21).

In Silico Prediction of OATP1B1 Inhibitors

A computational model in which inhibitors were discriminated from non-inhibitors was developed. The final model, after optimization through variable selection, was a single principal component OPLS-DA based on four descriptors, reflecting compound lipophilicity, polarity, size, and shape (Fig. 4a). The model shows that the inhibitors tend to be more lipophilic (AlogP descriptor), be larger (Mw descriptor) and display a larger polar surface area (PSA) than the non-inhibitors. In addition, the inhibitors display a lower value of the less interpretable shape descriptor, the Mean Square Distance Index (MSD), which is a topological distance descriptor normalized for size (36).

The OPLS-DA model successfully classified 81% of the inhibitors and 93% of the non-inhibitors in the test set

($n=48$) (Fig. 4b), indicating good applicability of the model. Transforming the OPLS-DA results to a multi-linear equation for the prediction of OATP1B1 inhibition resulted in OATP1B1 inhibitors being identified if the following sum results in a positive value:

$$OATP1B1_{inhib} = -0.167 + 0.001Mw - 3.234MSD$$
$$+ 0.062AlogP + 0.002PSA \quad (5)$$

Hence, negative values (<0) as output from Eq. 5 predict the compound to be a non-inhibitor of OATP1B1.

Concentration-Dependent Inhibition of Atorvastatin Uptake

For six selected OATP1B1 inhibitors and non-inhibitors, inhibition curves were derived using atorvastatin as the victim drug. As expected, inhibition curves could be derived and IC_{50} and K_i-values calculated for the five compounds previously classified as inhibitors in the screening assay (cyclosporin A, gemfibrozil, lopinavir, atazanavir, amprenavir). Fenofibrate did not inhibit atorvastatin uptake in the investigated concentration interval; hence, no IC_{50}- or K_i-values were calculated. For the three compounds used later on as calibrators in the *in vivo* predictions (see below), the expected inhibition ranking was obtained: cyclosporin A≫gemfibrozil≫fenofibrate. IC_{50}-values obtained were 1.88 μM for cyclosporin A and 156.2 μM for gemfibrozil, and K_i-values were 0.82 μM and 68.05 μM for cyclosporin A and gemfibrozil, respectively (Fig. 5, Table II) (37). For the remaining three HIV protease inhibitors, a concentration-dependent inhibition of atorvastatin uptake was observed, where lopinavir>atazanavir>amprenavir. The IC_{50} ranged between 0.74 μM (lopinavir) and 16.80 μM (amprenavir) and the K_i between 0.32 μM (lopinavir) and 9.52 μM (amprenavir) (Fig. 5, Table II).

Prediction of *In Vivo* Interactions

Recently, *in vitro–in vivo* extrapolation methods were proposed for prediction of clinical drug-drug interactions with drug-transporting proteins (3,22). These predictions are based on experimentally determined IC_{50}- and K_i-values, such as those presented for OATP1B1 in Table II and Fig. 5, and from which changes in drug exposure (R) are calculated as described in the methods section. Several variants for calculation of R-values have been proposed, where either IC_{50} or K_i values are used, and where different values are given to constants such as F_a and k_a in Eq. 4.

In the following, we investigate if calculated R-values could be used to predict previously observed clinical drug–
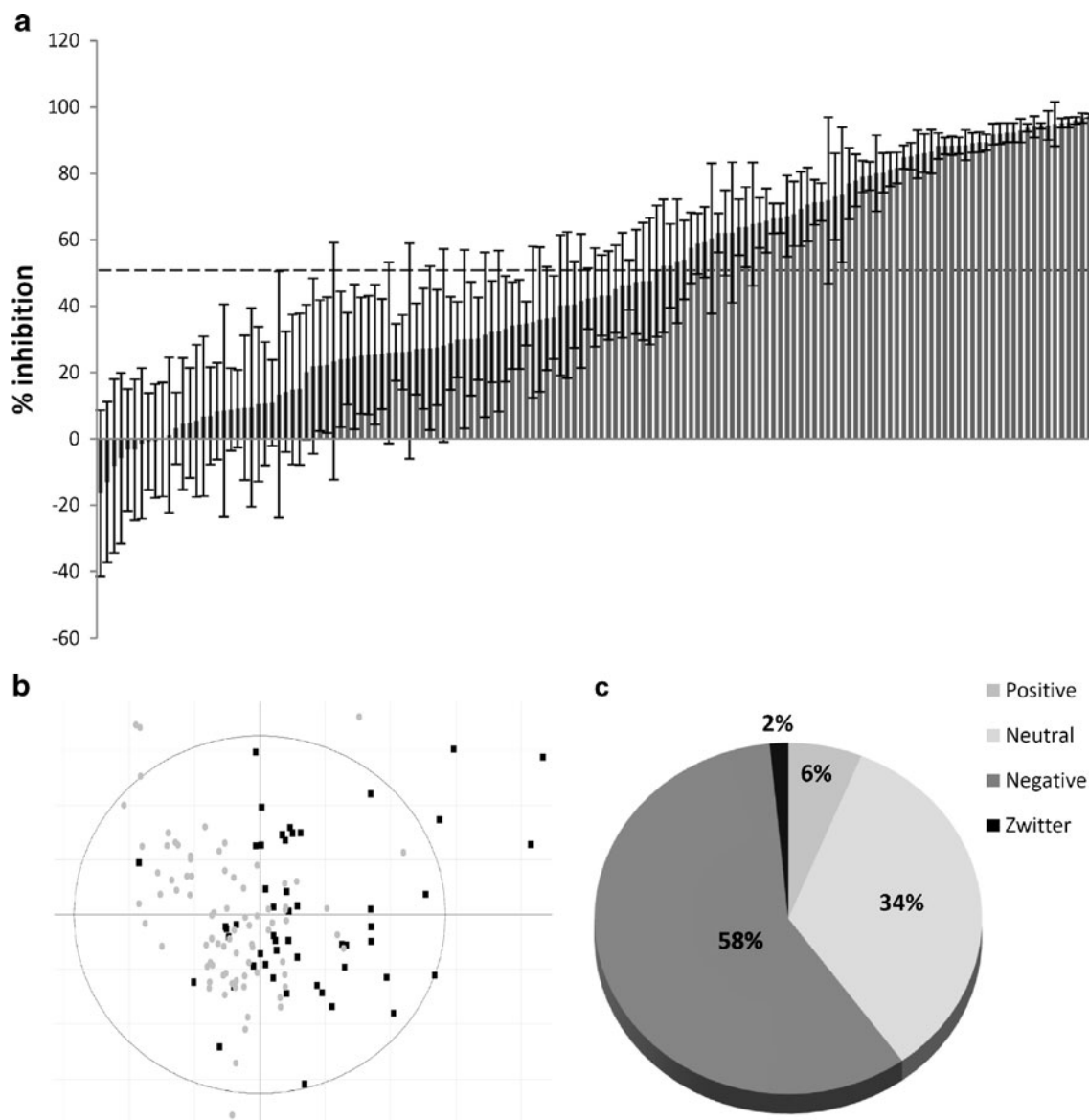
Fig. 3 Percentage inhibition of the dataset, as well as the compounds' properties of the OATP1B1 inhibitors identified. The mean percentage inhibition (± standard deviation) of all 146 of the compounds investigated (**a**). The 50% cut-off level is indicated by the *dashed line*. The inhibitors (*black squares*) and non-inhibitors (*grey dots*) superimposed on the oral drug space, presented as a PCA score plot (**b**). The first principal component (x-axis in the plot) is largely governed by the molecular size, which increases to the right. The second principal component (y-axis) is largely governed by the lipophilicity, which increases downwards. PC1 and PC2 describe 56% of the chemical variation of the oral drug space. The charge distribution of the inhibitors identified (**c**).

drug interactions (AUC-changes) with the compounds examined for atorvastatin inhibition in our study (Fig. 5, Table II). We also calculate *R*-values in eight different ways in order to investigate if any of the calculation methods provide better *in vitro–in vivo* predictions. For this purpose, we included three calibrators—cyclosporin A (a strong inhibitor), gemfibrozil (a moderate inhibitor) and fenofibate (a non-inhibitor)—to cover the range of the reported changes in the AUC *in vivo*. Using the maximal inhibitor concentration at the inlet of the liver ($I_{in,max}$) (obtained from Eq. 4 and variables shown in Table III), the predicted change in exposure (*R*) was calculated using Eqs. 2 and 3.

As can be seen in Table IV, the *R*-values varied depending on whether Eq. 2 (using IC_{50}) or Eq. 3 (using K_i) was used and on which values of F_a (the reported compound-specific value or assumed complete absorption) and k_a (0.03 or 0.1) were used in the calculations (Fig. 6, Tables III, IV). The mean *R*-value obtained for the strong OATP1B1 inhibitor cyclosporin A was 3.21 (range 1.46–7.15) and for the moderate inhibitor gemfibrozil was 1.11 (range 1.05–1.19) (Table IV, Fig. 7). The mean *R*-values for the three test compounds were as follows: lopinavir, 2.91 (range 1.76–4.58); atazanavir, 4.02 (range 2.06–7.49); and amprenavir 1.49 (range 1.19–1.95) (for all *R*-values as well as the

Table I Inhibition of Estradiol-17β-glucuronide Uptake by the Compounds Investigated

Compound	Inhibition %	SD % units	Compound	Inhibition %	SD % units	Compound	Inhibition %	SD % units
Taurolithocholate	97.8	1.1	Nicardipine	65.1	7.6	Mitoxantrone	27.2	18.2
Pitavastatin	97.4	0.6	Ivermectin	64.7	18.6	Chlorpromazine	27.1	13.8
Cyclosporine A	96.8	1.5	Progesterone	63.9	12.1	Amantadine	26.4	32.5
Atorvastatin	96.0	1.1	Saquinavir	63.8	8.5	Thioridazine	26.1	11.2
Rifamycin SV	95.4	1.5	Valsartan	62.2	21.1	Phalloidin	26.1	8.6
Estrone-3-sulphate	95.3	1.4	Diethylstilbestrol	62.1	12.9	Desipramine	25.9	27.3
Atazanavir	95.0	6.7	Adefovir	62.1	5.9	Tamoxifen	25.6	16.6
Silymarin	94.5	4.4	Olmesartan	60.4	22.7	Phenytoin	25.4	21.1
GF120918	94.4	0.9	Gemfibrozil	59.3	10.7	Valproic Acid	25.2	17.9
Bromosulfalein	94.1	3.2	Erythromycin	58.8	9.1	Prazosin	25.1	17.6
Fluo-3	93.9	1.2	Vinblastine	57.6	10.7	Trimethoprim	24.7	21.8
Taurocholate	93.0	3.6	Quinine	54.0	11.9	Amodiaquine	24.2	13.9
Glibenclamide	92.4	2.9	Ketoconazole	53.6	18.7	Chlorprothixene	24.0	20.5
Ritonavir	92.3	2.9	Pravastatin	52.2	12.6	Furosemide	23.4	35.7
Sulfasalazine	92.1	3.1	Candesartan	52.1	20.1	Astemizole	22.3	20.5
Dipyridamole	91.9	3.2	Ouabain	50.5	19.8	Tetracycline	22.1	19.7
Taurochenodeoxycholate	89.5	2.4	Disopyramide	47.5	19.1	Pioglitazone	21.9	26.5
Tipranavir	89.5	3.0	Isradipine	47.5	17.7	Chlorzoxazone	20.1	20.4
Cholecystokinin octapeptid	89.3	3.0	Ibuprofen	47.3	15.7	Fendiline	15.0	22.8
Indomethacin	88.6	4.5	Sotalol	46.4	7.6	Acarbose	14.9	22.6
MK-571	88.5	2.5	S-decyl-glutathione	46.3	15.8	1-methyl-4-phenylpyridinium	14.2	18.2
Repaglinide	88.4	2.9	Colchicine	45.2	13.2	Carbamazepine	13.3	37.2
Spironolactone	88.3	2.6	Quinidine	43.3	13.4	Bestatin	10.9	13.0
Rifampicin	88.3	3.9	Loratadine	43.2	12.1	Erlotinib	10.6	18.6
Benzbromarone	86.6	6.6	Terfenadine	42.7	14.8	Amitriptyline	10.5	23.4
Indocyanine green	86.1	5.8	Etoposide	42.2	9.2	Zidovudine	9.5	30.0
Lopinavir	85.8	7.3	Cholic acid	41.6	20.2	Cefadroxil	9.4	21.8
Morin	85.2	4.0	Irinotecan	40.5	13.1	Tolbutamide	9.1	11.8
Glycodeoxycholate	85.0	3.5	Verapamil	40.3	22.1	Penicillin G	8.8	12.4
Taurodeoxycholate	81.7	4.6	Cimetidine	40.3	21.2	Bupropion	8.5	32.1
Mifepristone	81.2	5.1	Carnitine	36.6	12.6	Valacyclovir	8.3	14.6
Glycochenodeoxycholate	80.2	5.9	Dextromethorphan	36.3	15.5	Nicotine	6.9	14.7
Fluvastatin	80.1	11.5	Digoxin	36.0	21.8	Flutamide	6.8	24.1
Amprenavir	79.3	4.3	Probenecid	35.2	22.8	Fenofibrate	5.4	23.0
Rosiglitazone	79.1	4.7	Naringenin	34.8	6.6	Ondansentron	4.8	16.6
Diclofenac	77.9	7.8	Phenformin	34.5	13.4	Lisinopril	4.6	19.8
Quercetin	77.0	10.8	Phenacetin	34.2	13.1	Diltiazem	3.2	10.8
Cerivastatin	73.6	20.4	Testosterone	33.2	15.9	Glipizide	1.1	23.4
Simvastatin	73.1	13.1	Loperamide	32.5	24.3	Sanguinarine chloride	-0.2	17.2
Indinavir	71.9	25.0	Clotrimazole	32.3	15.3	Chelerythrine	-0.7	17.2
N-methylnicotinamide	71.4	5.7	Lansoprazole	31.4	24.8	Quinone	-0.8	14.5
Rosuvastatin	71.4	6.8	Cefamandole	30.2	12.4	Chloroquine	-1.4	22.7
5-CFDA	70.7	11.1	Flupenthixol	30.2	17.1	Metformin	-3.3	21.3
Nystatin	69.3	11.2	P-aminohippuric acid	30.1	26.9	Celecoxib	-3.3	18.4
Estradiol-17-β-glucuronide	67.9	9.7	Isoniazid	29.9	11.4	Doxorubicin	-5.8	25.7
Reserpine	67.2	12.3	Doxazosin	28.8	14.0	Ofloxacin	-8.2	26.2
Lovastatin	66.5	4.5	Metoprolol	28.1	29.1	Levothyroxin	-13.1	24.3
Glycocholic acid hydrate	66.4	4.5	Baicalin	27.6	17.4	Phenylethyl isothiocyanate	-16.4	25.1
Glycyrrhizic acid	65.8	9.7	Methotrexate	27.4	24.7			

Inhibition > 90%	Inhibition 50-90%	Inhibition < 50%

corresponding letter used, see Table IV). Of the eight different R-values calculated, the most pronounced difference between the groups of non-inhibitors and inhibitors was observed for R-value H with a 6.3-fold difference between the highest and lowest inhibitor and non-inhibitor, respectively (Fig. 6a). R-value H was calculated using the method described by Hirano and co-workers (22); there, Eq. 3 (based on a K_i-value) is used together with a default value of k_a equal to 0.1 an F_a equal to 1. In addition, for R-value B (the R-calculation proposed by the International Transporter Consortium (3)), an F_a equal to 1 is used. However, the major differences when compared to the

a

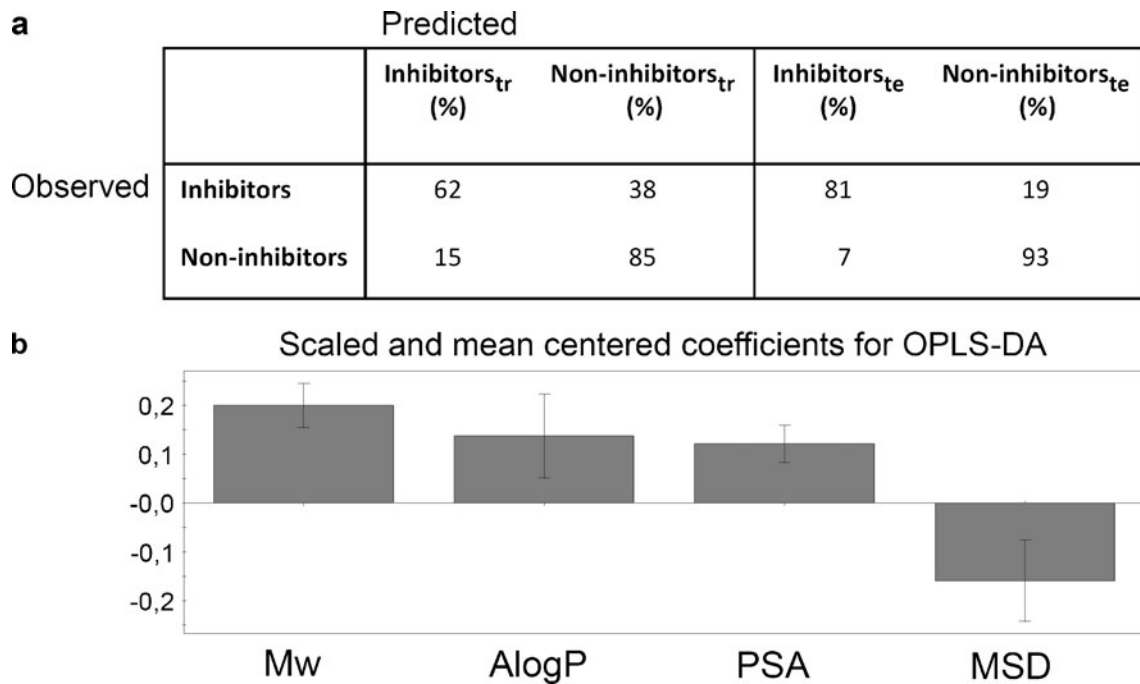|	Predicted			
	Inhibitors$_{tr}$ (%)	Non-inhibitors$_{tr}$ (%)	Inhibitors$_{te}$ (%)	Non-inhibitors$_{te}$ (%)
Observed **Inhibitors**	62	38	81	19
Non-inhibitors	15	85	7	93

b

Fig. 4 Performance of the *in silico* model. Accuracy of the prediction of OATP1B1 inhibition for the training and test sets (left and right panels, respectively) (**a**). The OPLS-DA coefficients show that the molecular weight (Mw), polar surface area (PSA) and lipophilicity (AlogP) are positive for OATP1B1 inhibition and that the mean square distance (MSD; a Balaban index descriptor) is negative for OATP1B1 inhibition (**b**).
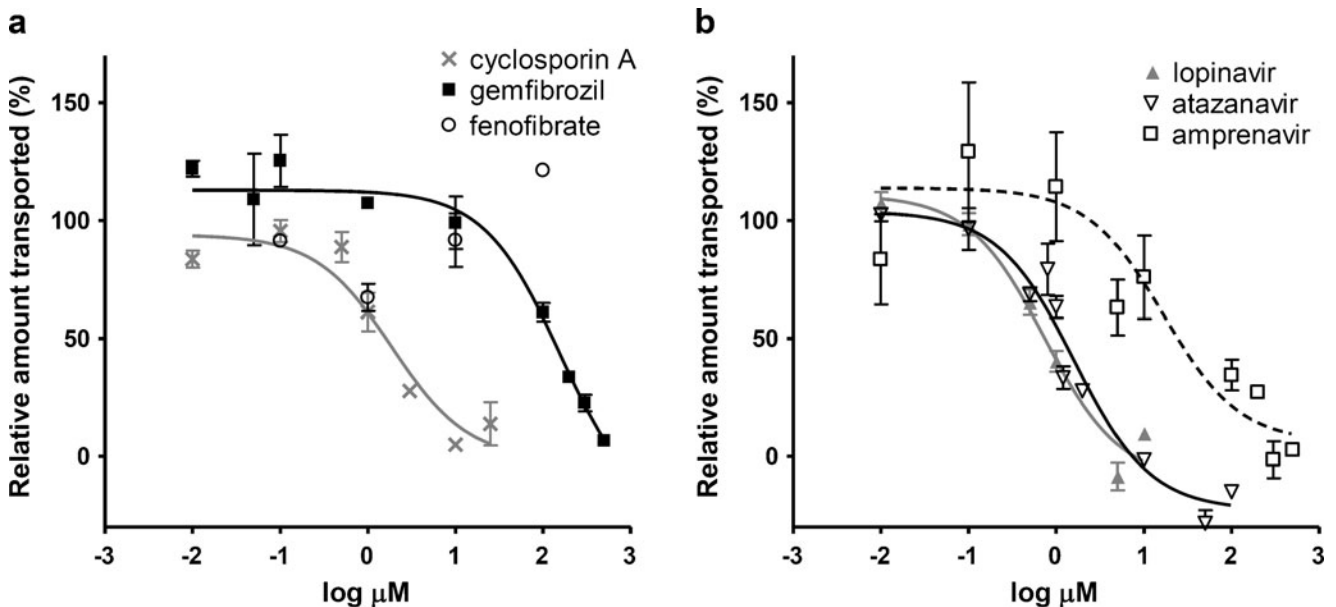

Fig. 5 Inhibition of OATP1B1-mediated atorvastatin uptake in HEK293 cells stably expressing the OATP1B1 transporter for the three calibrators: cyclosporin A, gemfibrozil, fenofibrate (**a**) and for the three protease inhibitors investigated: lopinavir, atazanavir, amprenavir (**b**). HEK293-OATP1B1 and mock-transfected cells grown in 24-well plates were incubated with 1 μM atorvastatin together with increasing concentrations of the potential inhibitors for 2 min at 37°C. The intracellular accumulation of atorvastatin was measured using UPLC-MS/MS analysis. On the y-axis, the relative amount transported in comparison to a non-inhibitor control is shown as a percentage $\pm$ standard deviation ($n = 4$, for 200 and 500 μM amprenavir $n = 2$). At each inhibitor concentration, the passive uptake of atorvastatin in the mock cells was subtracted from the total atorvastatin uptake in the OATP1B1-expressing cells. On the x-axis, the inhibitor concentration is shown as log μM. For fenofibrate, no curve could be generated, so only the values obtained are shown.

Table II IC$_{50}$- and K$_i$-Values Obtained for the Six Compounds Investigated Using HEK293-OATP1B1 Cells and Atorvastatin as the Substrate, Relative Changes in the AUC for Atorvastatin and Rosuvastatin (as Reviewed by Kalliokoski and Niemi [37] or Reported by [27,43,51])

	IC$_{50}$ (μM)	K$_i$ (μM)	Fold AUC change Atorvastatin	Fold AUC change Rosuvastatin
Cyclosporin A	1.88	0.82	10.5 (7.4–15.3)	7.1
Gemfibrozil	156.2	68.05	1.2	1.9
Fenofibrate	–	–	–	1.1
Lopinavir	0.74	0.32	–	2.1
Atazanavir	1.61	0.91	–	3.1
Amprenavir	16.80	9.52	–	1.1[a]

[a] The prodrug Fosamprenavir was used in the study

calculation of *R*-value H are that for *R*-value B, the IC$_{50}$-value is used instead of K$_i$, and a default value of k$_a$ equal to 0.03 is used instead of 0.1. This results in lower *R*-values than the ones obtained with the method described by Hirano *et al.* [22], with a 2.3-fold difference between the highest and lowest calculated *R*-value, in comparison to a 6.3-fold difference for *R*-value H (Fig. 6).

DISCUSSION

In this paper, we investigated OATP1B1 inhibition for a dataset of 146 compounds within the chemical space of oral drugs and enriched with compounds considered likely to interact with OATP1B1. Through this approach, a relatively large number of inhibitors was identified (42%), supporting the notion that OATP1B1 should be considered in predictions of clinical drug–drug interactions [6,7,14,15],

Table III Variables Used for the Calculation of *R*-Values

	I$_{max}$[a] (μM)	F$_a$[b]	Dose[c] (mg)	F$_u$[d]
Cyclosporin A	1.37	0.5	886.2	0.1
Gemfibrozil	99.9	0.98	600	0.05
Fenofibrate	29.8	0.81	300	0.01
Lopinavir	15.4	na	400	0.02
Atazanavir	4.47	0.68	400	0.14
Amprenavir[e]	11.2	0.9	600	0.1

na not available

[a] Maximum systemic plasma concentration of the inhibitor, obtained from [23–28]

[b] Fraction of the inhibitor dose absorbed. Here, the maximum oral bioavailability, as obtained from [23–25], is displayed

[c] Inhibitor dose for each occasion on which a dose was given, obtained from [23–28]

[d] Fraction of the inhibitor that is unbound, obtained from [3,23,24]

[e] I$_{max}$ and the dose, recalculated from Fosamprenavir data

particularly if the drug is uncharged or has a negative charge (Fig. 3c) [4,5].

Three compounds that have previously been reported to interact with OATP1B1 (penicillin G, phalloidin, levothyroxine [31–33]) were not identified as inhibitors according to our definition (>50% inhibition at 20 µM). When investigated at higher concentrations, an increased inhibition of OATP1B1-mediated E17βG uptake was observed for all three of the compounds. Hence, we conclude that although these compounds were not defined as OATP1B1 inhibitors in our study, they could be classified as inhibitors if a less stringent definition is used.

Interestingly, among the 22 novel OATP1B1 inhibitors identified in this study, we found compounds known to be substrates or inhibitors for other transporters, e.g. GF120918 and ivermectin, both of which are reported to interact with MDR1 and also with other ABC transporters (http://125.206.112.67/tp-search) [20]. One inhibitor, diclofenac, was confirmed to be an OATP1B1 inhibitor during the finalization of this manuscript by Kindla and co-workers [16]. In addition to the novel inhibitors that we identified, we confirm the hypothesis that, e.g., indomethacin, spironolactone, tipranavir, taurochenodeoxycholate and taurodeoxycholate interact with the OATP1B1 transporter, as suggested by previous studies and investigations using human hepatocytes. Tipranavir, which inhibited OATP1B1 to approximately 90% here, had been suggested to be an OATP1B1 inhibitor in an earlier *in vivo* study [38]. Both for tipranavir and for the other novel OATP1B1 inhibitors identified here, further investigation will be needed to confirm our findings and to establish the importance of OATP1B1 in DDIs in comparison to the relative importance of other transporters and metabolizing enzymes involved in the pharmacokinetics of these compounds.

We used our experimental data to analyze OATP1B1 inhibitors and non-inhibitors from a molecular perspective using both single correlations between inhibition and molecular properties and a multivariate data analysis. We found that OATP1B1 inhibitors tend to be more lipophilic,

Table IV Calculated *R*-Values

	Eq. 2 $R = 1 + fu* \frac{I_{in,max}}{IC_{50}}$				Eq. 3 $R = 1 + fu* \frac{I_{in,max}}{K_i}$				Average
	$k_a = 0.03^a$		$k_a = 0.1^a$		$k_a = 0.03^a$		$k_a = 0.1^a$		
	F_a published value[b] A	$F_a = 1$ B	F_a published value[b] C	$F_a = 1$ D	F_a published value[b] E	$F_a = 1$ F	F_a published value[b] G	$F_a = 1$ H	
Cyclosporin A[c]	1.46	1.86	2.38	3.68	2.07	2.96	4.16	7.15	3.21
Gemfibrozil	1.05	1.05	1.08	1.08	1.11	1.11	1.19	1.19	1.11
Fenofibrate	–	–	–	–	–	–	–	–	–
Lopinavir	1.76	1.76	2.56	2.56	2.74	2.74	4.58	4.58	2.91
Atazanavir	2.06	2.38	3.63	4.68	2.87	3.43	5.64	7.49	4.02
Amprenavir[d]	1.19	1.21	1.49	1.54	1.34	1.37	1.87	1.95	1.49

[a] Absorption rate constant obtained from (22,29)

[b] Maximum percentage absorbed or the oral availability as obtained from (22–25,29). For lopinavir, no data was available, hence $F_a = 1$ was used

[c] Cyclosporin A dose: 12.66 mg/kg/day for an individual with a weight of 70 kg

[d] I_{max} and dose (used for the calculation of $I_{In,max}$), recalculated from Fosamprenavir data
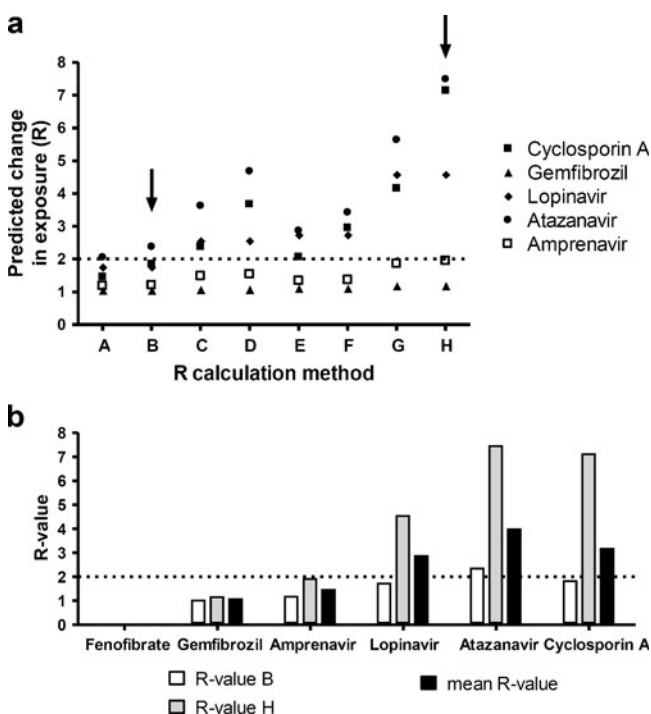

Fig. 6 Variation in the range of calculated *R*-values (predicted change in exposure) obtained by applying different equations (Eq. 2 using IC_{50} or Eq. 3 using K_i), with different k_a (0.03 or 0.1) and different F_a (literature values (see Table IV) or 1) (**a**). All *R*-values, as well as the corresponding letter used, can be found in Table IV. The *R* calculation methods suggested by the International Transporter Consortium (3) (B) and Hirano *et al.* (22) (H) are indicated here with *black arrows*. An overview of the *R*-values calculated for each compound using the methods suggested by the International Transporter Consortium (3) (B) with *white bars* and by Hirano and coworkers (22) (H) with *grey bars* (**b**). The mean *R*-values based on all eight values calculated (*R*-values A–H) for each compound are shown as *black bars*.

be larger, display a larger polar surface area, and be enriched with regard to anionic charge in comparison to non-inhibitors. Comparing the molecular properties defining OATP1B1 inhibitors in this study with those obtained in investigations of other transport proteins reveals that several molecular properties are shared between inhibitors of different transport proteins. For instance, lipophilicity seems to be a general property of transporter inhibitors (18–21,39). The accuracy of the classification of inhibitors and non-inhibitors obtained using the PLS-DA model introduced here was similar to that of models developed previously by our group for the OCT1, MRP2, MDR1 and BCRP transporters (18–21). Through the use of these and
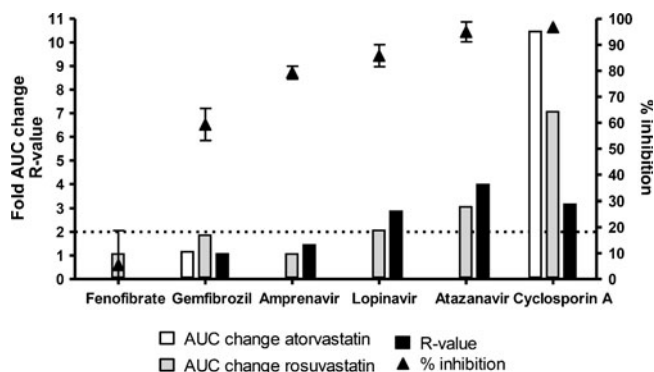

Fig. 7 Comparison of reported AUC changes for atorvastatin (two compounds) and rosuvastatin (six compounds) (27,37,43,51) with the mean *R*-extrapolation values based on the inhibition curves obtained. The percentage inhibition ± standard deviation in the OATP1B1 screening assay is displayed as triangles. For fenofibrate, no IC_{50} value was obtained in the investigated concentration interval, so no *R*-value could be calculated. For the values used, see Tables I, II, and IV. The relative changes in AUC for atorvastatin and rosuvastatin were taken from (27,37,43,51) and from references therein.

similar *in silico* models, it is now possible to predict the inhibition pattern of molecular structures within the chemical space of drug-like molecules and to identify specific and overlapping inhibitors (20). In 2005, Chang and co-workers published a substrate pharmacophore for OATP1B1 (40), which we also examined. However, neither the pharmacophore nor the predictive quantitative model approach that they adopted was successful in predicting our inhibition data. The inability to generate these models with our data was not surprising, given the larger size ($n=146$) and higher structural diversity of our dataset in comparison to that investigated by Chang *et al.* ($n=19$). We conclude that the development of global pharmacophore models for structurally diverse inhibitors will require structural information about the binding site that is not currently available for these integral membrane proteins.

Many groups have reported that statins, in particular, interact with the OATP1B1 transporter e.g. (22,41,42), and therefore this class of compounds was studied in further detail in this paper. All of the statins investigated here were identified as OATP1B1 inhibitors; the same was observed for the seven protease inhibitors examined. This is in agreement with the results available in the literature, where the more polar statins, especially, have been reported to be dependent on active uptake into the liver (mainly mediated by OATPs) and where several clinical DDIs involving statins and protease inhibitors have been described (7,27,28,43).

In this investigation, we have further examined the interaction potential and methods for *in vivo* prediction of three protease inhibitors using atorvastatin as a substrate. Atorvastatin was chosen since it is predominantly transported into hepatocytes by OATP1B1. Importantly, three compounds were used for calibration (cf. (3)), cyclosporin A (a strong OATP1B1 inhibitor increasing the plasma concentration of atorvastatin and rosuvastatin in humans by a factor of 10.5 and 7.1, respectively), gemfibrozil (a moderate OATP1B1 inhibitor increasing the AUC for atorvastatin and rosuvastatin by 1.2 and 1.9 times, respectively), and fenofibrate (a non-inhibitor *in vivo* of rosuvastatin); for all changes in the AUC, see the review of Kalliokoski (37) and references therein. Thus, the *in vivo* ranking was comparable to the ranking observed here *in vitro*, both for the IC_{50} values (Fig. 5a) and for the mean predicted *R*-values (Fig. 7).

Our first question was whether the calculated *R*-values could classify the chosen calibrators into interacting and non-interacting drugs. In the recent paper by Giacomini and co-workers, an $R>2$ was suggested as the threshold for an *in vivo* interaction (3). As can be seen from Table V and Fig. 6, this threshold should not be applied to all proposed calculations of the *R*-value. However, for all predictions the strong inhibitor cyclosporin A had a higher *R*-value than

the moderate inhibitor gemfibrozil. Hence, our conclusion is that the *R*-values correctly classified the compounds into interacting and non-interacting drugs, but that an *R*-value of larger than 2 is not always applicable.

Our next question was if the *R*-values also could predict the magnitude of the cyclosporin A/gemfibrozil-statin interactions. A mean *R*-value of 3.21 was obtained for the cyclosporin A-statin interaction and a larger *R*-value might have been expected from the large effect on the AUC of atorvastatin and rosuvastatin, respectively. However, cyclosporin A is a multispecific inhibitor that interacts with several transporters and metabolizing enzymes (including cytochromes P450s that are responsible for statin metabolism) (3,44,45) and therefore, the large effects of the two statins caused by cyclosporin A are not only a reflection of the OATP1B1 interaction, but of the overall effect on several transporters and enzymes *in vivo*. For gemfibrozil the minor change in predicted atorvastatin exposure (mean *R*-value of 1.11) is in agreement with the low increase in the AUC observed for the gemfibrozil-atorvastatin interaction in human studies (1.2-fold increase in AUC) (Fig. 7, Table II) (46). In addition, it is also in agreement with other *in vitro–in vivo* extrapolations made previously (22). For gemfibrozil-rosuvastatin interactions, a slightly larger AUC increase of 1.9-fold has been observed (see Table II). This difference is probably the result of slightly different substrate/inhibition profiles for the interacting drugs (47–49). In summary, this shows that predicting the magnitude of interactions based on *R*-values is more difficult than classifying compounds as interacting or non-interacting. For more quantitative predictions the contribution of additional factors, such as drug metabolizing enzymes and multiple transporters needs to be considered.

To investigate to what extent it is possible to classify and predict the magnitude of DDIs, the three test compounds lopinavir, atazanavir and amprenavir were used. For these compounds, limited clinical data is available regarding drug transporters and transporter-mediated DDIs with atorvastatin. Concomitant treatment with these compounds and rosuvastatin resulted in increased rosuvastatin plasma concentrations for lopinavir and atazanavir (with a 2.1 and 3.1-fold increase, respectively (27,43)) suggesting involvement of transporter inhibition, most likely of OATP1B1. For amprenavir no increase was observed in the rosuvastatin plasma concentration (43). The *R*-values for the three protease inhibitors suggest a more than 2-fold change in the exposure of atorvastatin for patients concomitantly treated with lopinavir (six out of eight *R*-values >2) and atazanavir (all eight *R*-values >2), but not amprenavir (all eight *R*-values <2) (Table IV, Fig. 7), thereby correctly classifying these three compounds into interacting/non-interacting drugs. The clinical data for rosuvastatin-lopinavir or rosuvastatin-atazanavir DDIs

agree fairly well with the predictions made here. The reported changes in the AUC are within the range of the predicted *R*-values and the average *R*-values are approximately 30% higher than the AUC-change. We conclude that these three test compounds, too, could be correctly classified as inhibitors/non-inhibitors using R calculations.

Several different values for the various parameters required for the calculation of *R*-values have been suggested. How does the *R*-value vary with different choices of values? To investigate this issue, we calculated *R*-values using eight different combinations of variables. Of these eight *R*-values, the most pronounced difference between the groups of non-inhibitors and inhibitors was observed for *R*-value H (Table IV, Fig. 6a). Hence, according to our data, this combination of values and method of calculation can be considered as the most discriminating for the classification of compounds. In addition, *R*-value H also gives the highest *R*-values for all compounds analyzed and can therefore be considered to represent a "worst case scenario" prediction. If we take all five compounds into consideration, and disregard potential interactions with other transporters or enzymes, then *R*-value H (Table IV) will also be closer to the actual change in the AUC for rosuvastatin. Surprisingly, using a method favored elsewhere (3), give lower *R*-values and a poorer separation between the groups of inhibitors and non-inhibitors, as compared to *R*-value H. Besides the considerable impact of the variables selected and the method used for the calculation, also different *in vitro* methods can affect the obtained *R*-values. This becomes clear when comparing the *R*-values obtained here for lopinavir with those calculated in reference (3). In this case, the discrepancy in the *R*-values (*R*-value B 1.76 *vs* 9.2) is solely dependent on the differences in IC_{50} obtained in the various studies and cell systems used. Hence, the possibility of the substrate, concentration or *in vitro* system used having an impact on the calculations cannot be excluded. Thus, calibration of the range and threshold of the *R*-value in each experimental system is a preferred approach.

In summary our results clearly stress the importance of using the reference inhibitors derived from known and well-defined clinical interactions as calibrators, and they underscore the need for a thorough analysis of the extrapolation method used instead of focusing on a proposed threshold of, e.g., greater than two-fold change in exposure. By taking these precautions, over or underestimations of possible interactions are more likely to be avoided, and hence a better prediction of the clinical situation ought to be obtained. This reasoning is analogous to that applied in other *in vitro–in vivo* predictions, such as *in vivo* absorption predictions from Caco-2 cell monolayer permeability experiments, where the use of reference drugs as calibrators can account for large variations in the observed cut-off values in different laboratories (50).

CONCLUSIONS

In this study, we identified 65 OATP1B1 inhibitors, of which 22 had not been identified previously as interacting with the OATP1B1 transporter. To our knowledge, this is the most comprehensive investigation of OATP1B1 inhibition conducted to date, as well as the first global computational classification model developed for the prediction of inhibition of the OATP1B1 transporter. Furthermore, we applied newly recommended *in vitro–in vivo* extrapolation methods for the prediction of clinical DDIs with transport proteins (3). Our classification of OATP1B1 *in vivo* interactions was in good agreement with reported clinical data and emphasizes the need to include compounds whose clinical inhibition pattern is known to calibrate the *R*-value. Awareness of how the different variables influence calculation of the *R*-value is essential. We believe that the results obtained in this work, together with previous studies on hepatic transporter interactions, will contribute to the ongoing discussion on the applications and development of relevant predictive preclinical tools.

ACKNOWLEDGMENTS & DISCLOSURES

REFERENCES

1. Hilgendorf C, Ahlin G, Seithel A, Artursson P, Ungell AL, Karlsson J. Expression of thirty-six drug transporter genes in human intestine, liver, kidney, and organotypic cell lines. Drug Metab Dispos. 2007;35(8):1333–40.

2. Hsiang B, Zhu Y, Wang Z, Wu Y, Sasseville V, Yang WP, *et al.* A novel human hepatic organic anion transporting polypeptide (OATP2). Identification of a liver-specific human organic anion transporting polypeptide and identification of rat and human hydroxymethylglutaryl-CoA reductase inhibitor transporters. J Biol Chem. 1999;274(52):37161–8.

3. Giacomini KM, Huang SM, Tweedie DJ, Benet LZ, Brouwer KL, Chu X, *et al.* Membrane transporters in drug development. Nat Rev Drug Discov. 2010;9(3):215–36.

4. Cui Y, Konig J, Leier I, Buchholz U, Keppler D. Hepatic uptake of bilirubin and its conjugates by the human organic anion transporter SLC21A6. J Biol Chem. 2001;276(13):9626–30.

5. Tirona RG, Leake BF, Wolkoff AW, Kim RB. Human organic anion transporting polypeptide-C (SLC21A6) is a major determinant of rifampin-mediated pregnane X receptor activation. J Pharmacol Exp Ther. 2003;304(1):223–8.

6. Kajosaari LI, Niemi M, Neuvonen M, Laitila J, Neuvonen PJ, Backman JT. Cyclosporine markedly raises the plasma concentrations of repaglinide. Clin Pharmacol Ther. 2005;78(4):388–99.

7. Neuvonen PJ, Niemi M, Backman JT. Drug interactions with lipid-lowering drugs: mechanisms and clinical relevance. Clin Pharmacol Ther. 2006;80(6):565–81.

8. Treiber A, Schneiter R, Hausler S, Stieger B. Bosentan is a substrate of human OATP1B1 and OATP1B3: inhibition of hepatic uptake as the common mechanism of its interactions with cyclosporin A, rifampicin, and sildenafil. Drug Metab Dispos. 2007;35(8):1400–7.

9. Mikkaichi T, Suzuki T, Tanemoto M, Ito S, Abe T. The organic anion transporter (OATP) family. Drug Metab Pharmacokinet. 2004;19(3):171–9.

10. Yamaguchi H, Okada M, Akitaya S, Ohara H, Mikkaichi T, Ishikawa H, et al. Transport of fluorescent chenodeoxycholic acid via the human organic anion transporters OATP1B1 and OATP1B3. J Lipid Res. 2006;47(6):1196–202.

11. Liu L, Cui Y, Chung AY, Shitara Y, Sugiyama Y, Keppler D, et al. Vectorial transport of enalapril by Oatp1a1/Mrp2 and OATP1B1 and OATP1B3/MRP2 in rat and human livers. J Pharmacol Exp Ther. 2006;318(1):395–402.

12. Kindla J, Fromm MF, Konig J. In vitro evidence for the role of OATP and OCT uptake transporters in drug–drug interactions. Expert Opin Drug Metab Toxicol. 2009;5(5):489–500.

13. Matsushima S, Maeda K, Ishiguro N, Igarashi T, Sugiyama Y. Investigation of the inhibitory effects of various drugs on the hepatic uptake of fexofenadine in humans. Drug Metab Dispos. 2008;36(4):663–9.

14. Simonson SG, Raza A, Martin PD, Mitchell PD, Jarcho JA, Brown CD, et al. Rosuvastatin pharmacokinetics in heart transplant recipients administered an antirejection regimen including cyclosporine. Clin Pharmacol Ther. 2004;76(2):167–77.

15. van Giersbergen PL, Treiber A, Schneiter R, Dietrich H, Dingemanse J. Inhibitory and inductive effects of rifampin on the pharmacokinetics of bosentan in healthy subjects. Clin Pharmacol Ther. 2007;81(3):414–9.

16. Kindla J, Muller F, Mieth M, Fromm MF, Konig J. Influence of non-steroidal anti-inflammatory drugs on organic anion transporting polypeptide (OATP)1B1- and OATP1B3-mediated drug transport. Drug Metab Dispos. 2011;39(6):1047–53.

17. Poirier A, Funk C, Lave T, Noe J. New strategies to address drug–drug interactions involving OATPs. Curr Opin Drug Discov Dev. 2007;10(1):74–83.

18. Ahlin G, Karlsson J, Pedersen JM, Gustavsson L, Larsson R, Matsson P, et al. Structural requirements for drug inhibition of the liver specific human organic cation transport protein 1. J Med Chem. 2008;51(19):5932–42.

19. Matsson P, Englund G, Ahlin G, Bergstrom CA, Norinder U, Artursson P. A global drug inhibition pattern for the human ATP-binding cassette transporter breast cancer resistance protein (ABCG2). J Pharmacol Exp Ther. 2007;323(1):19–30.

20. Matsson P, Pedersen JM, Norinder U, Bergstrom CA, Artursson P. Identification of novel specific and general inhibitors of the three major human ATP-binding cassette transporters P-gp, BCRP and MRP2 among registered drugs. Pharm Res. 2009;26(8):1816–31.

21. Pedersen JM, Matsson P, Bergstrom CA, Norinder U, Hoogstraate J, Artursson P. Prediction and identification of drug interactions with the human ATP-binding cassette transporter multidrug-resistance associated protein 2 (MRP2; ABCC2). J Med Chem. 2008;51(11):3275–87.

22. Hirano M, Maeda K, Shitara Y, Sugiyama Y. Drug–drug interaction between pitavastatin and various drugs via OATP1B1. Drug Metab Dispos. 2006;34(7):1229–36.

23. Dollery CT, editor. Therapeutic drugs. 2. ed. Edinburgh: Churchill Livingstone; 1999.

24. Goodman LS, Gilman A, Brunton LL, editors. Goodman & Gilman's the pharmacological basis of therapeutics [Electronic resource]. New York: McGraw-Hill; 2005.

25. Busti AJ, Hall RG, Margolis DM. Atazanavir for the treatment of human immunodeficiency virus infection. Pharmacotherapy. 2004;24(12):1732–47.

26. Asberg A, Hartmann A, Fjeldsa E, Bergan S, Holdaas H. Bilateral pharmacokinetic interaction between cyclosporine A and atorvastatin in renal transplant recipients. Am J Transplant. 2001;1(4):382–6.

27. Kiser JJ, Gerber JG, Predhomme JA, Wolfe P, Flynn DM, Hoody DW. Drug/Drug interaction between lopinavir/ritonavir and rosuvastatin in healthy volunteers. J Acquir Immune Defic Syndr. 2008;47(5):570–8.

28. van der Lee MJ, Blenke AA, Rongen GA, Verwey-van Wissen CP, Koopmans PP, Pharo C, et al. Interaction study of the combined use of paroxetine and fosamprenavir-ritonavir in healthy subjects. Antimicrob Agents Chemother. 2007;51(11):4098–104.

29. Obach RS, Walsky RL, Venkatakrishnan K, Gaman EA, Houston JB, Tremaine LM. The utility of in vitro cytochrome P450 inhibition data in the prediction of drug–drug interactions. J Pharmacol Exp Ther. 2006;316(1):336–48.

30. Vieth M, Siegel MG, Higgs RE, Watson IA, Robertson DH, Savin KA, et al. Characteristic physical properties and structural fragments of marketed oral drugs. J Med Chem. 2004;47(1):224–32.

31. Abe T, Kakyo M, Tokui T, Nakagomi R, Nishio T, Nakai D, et al. Identification of a novel gene family encoding human liver-specific organic anion transporter LST-1. J Biol Chem. 1999;274(24):17159–63.

32. Fehrenbach T, Cui Y, Faulstich H, Keppler D. Characterization of the transport of the bicyclic peptide phalloidin by human hepatic transport proteins. Naunyn Schmiedebergs Arch Pharmacol. 2003;368(5):415–20.

33. Tamai I, Nezu J, Uchino H, Sai Y, Oku A, Shimane M, et al. Molecular identification and characterization of novel members of the human organic anion transporter (OATP) family. Biochem Biophys Res Commun. 2000;273(1):251–60.

34. Bachmakov I, Glaeser H, Fromm MF, Konig J. Interaction of oral antidiabetic drugs with hepatic uptake transporters: focus on organic anion transporting polypeptides and organic cation transporter 1. Diabetes. 2008;57(6):1463–9.

35. Kalliokoski A, Backman JT, Neuvonen PJ, Niemi M. Effects of the SLCO1B1*1B haplotype on the pharmacokinetics and pharmacodynamics of repaglinide and nateglinide. Pharmacogenet Genomics. 2008;18(11):937–42.

36. Balaban AT. Topological indices based on topological distances in molecular graphs. Pure & Appl Chem. 1983;55(2):199–206.

37. Kalliokoski A, Niemi M. Impact of OATP transporters on pharmacokinetics. Br J Pharmacol. 2009;158(3):693–705.

38. Pham PA, la Porte CJ, Lee LS, van Heeswijk R, Sabo JP, Elgadi MM, et al. Differential effects of tipranavir plus ritonavir on atorvastatin or rosuvastatin pharmacokinetics in healthy volunteers. Antimicrob Agents Chemother. 2009;53(10):4385–92.

39. Kido Y, Matsson P, Giacomini KM. Profiling of a prescription drug library for potential renal drug–drug interactions mediated by the organic cation transporter 2. J Med Chem. 2011;54(13):4548–58.

40. Chang C, Pang KS, Swaan PW, Ekins S. Comparative pharmacophore modeling of organic anion transporting polypeptides: a meta-analysis of rat Oatp1a1 and human OATP1B1. J Pharmacol Exp Ther. 2005;314(2):533–41.

41. Kivisto KT, Niemi M. Influence of drug transporter polymorphisms on pravastatin pharmacokinetics in humans. Pharm Res. 2007;24(2):239–47.

42. Noe J, Portmann R, Brun ME, Funk C. Substrate-dependent drug–drug interactions between gemfibrozil, fluvastatin and other organic anion-transporting peptide (OATP) substrates on OATP1B1, OATP2B1, and OATP1B3. Drug Metab Dispos. 2007;35(8):1308–14.

43. Busti AJ, Bain AM, Hall 2nd RG, Bedimo RG, Leff RD, Meek C, et al. Effects of atazanavir/ritonavir or fosamprenavir/ritonavir on the pharmacokinetics of rosuvastatin. J Cardiovasc Pharmacol. 2008;51(6):605–10.

44. Kullak-Ublick GA, Stieger B, Hagenbuch B, Meier PJ. Hepatic transport of bile salts. Semin Liver Dis. 2000;20(3):273–92.

45. Pal D, Mitra AK. MDR- and CYP3A4-mediated drug-herbal interactions. Life Sci. 2006;78(18):2131–45.

46. Backman JT, Luurila H, Neuvonen M, Neuvonen PJ. Rifampin markedly decreases and gemfibrozil increases the plasma concentrations of atorvastatin and its metabolites. Clin Pharmacol Ther. 2005;78(2):154–67.

47. Ho RH, Tirona RG, Leake BF, Glaeser H, Lee W, Lemke CJ, et al. Drug and bile acid transporters in rosuvastatin hepatic uptake: function, expression, and pharmacogenetics. Gastroenterology. 2006;130(6):1793–806.

48. Grube M, Kock K, Oswald S, Draber K, Meissner K, Eckel L, et al. Organic anion transporting polypeptide 2B1 is a high-affinity transporter for atorvastatin and is expressed in the human heart. Clin Pharmacol Ther. 2006;80(6):607–20.

49. Kameyama Y, Yamashita K, Kobayashi K, Hosokawa M, Chiba K. Functional characterization of SLCO1B1 (OATP-C) variants, SLCO1B1*5, SLCO1B1*15 and SLCO1B1*15+C1007G, by using transient expression systems of HeLa and HEK293 cells. Pharmacogenet Genomics. 2005;15(7):513–22.

50. Artursson P, Palm K, Luthman K. Caco-2 monolayers in experimental and theoretical predictions of drug transport. Adv Drug Deliv Rev. 2001;46(1–3):27–43.

51. Martin PD, Dane AL, Schneck DW, Warwick MJ. An open-label, randomized, three-way crossover trial of the effects of coadministration of rosuvastatin and fenofibrate on the pharmacokinetic properties of rosuvastatin and fenofibric acid in healthy male volunteers. Clin Ther. 2003;25(2):459–71.